Ji *et al. Microstructures* **2025**, *5*, 2025072
DOI: 10.20517/microstructures.2024.165

Microstructures

Research Article

Open Access

Fluorine-doped titanium dioxide nanorod arrays for efficient photoelectrochemical water splitting

Ming-Hao Ji[1,4#], Wen Chen[1,2,4#], Ao-Sheng She[1,2,4], Yang Yang[1,3,4], Hao-Yan Shi[1,4], Hai-Long Wang[1,4], Ke-Xian Li[1,2,4], Xiu-Mei Lin[5], Yan-Xin Chen[1,2,4,6], Can-Zhong Lu[1,2,4,6]

[1]State Key Laboratory of Structural Chemistry, Fujian Institute of Research on the Structure of Matter, Chinese Academy of Sciences, Fuzhou 350002, Fujian, China.
[2]College of Chemistry, Fuzhou University, Fuzhou 350116, Fujian, China.
[3]College of Chemistry and Materials Science, Fujian Normal University, Fuzhou 350108, Fujian, China.
[4]Xiamen Key Laboratory of Rare Earth Photoelectric Functional Materials, Xiamen Institute of Rare-earth Materials, Haixi Institutes, Chinese Academy of Sciences, Xiamen 361021, Fujian, China.
[5]College of Chemistry, Chemical Engineering and Environment, Minnan Normal University, Zhangzhou 363000, Fujian, China.
[6]Fujian Science & Technology Innovation Laboratory for Optoelectronic Information of China, Fuzhou 350108, Fujian, China.
[#]These authors contributed equally to this work.

Correspondence to: Prof. Yan-Xin Chen and Prof. Can-Zhong Lu, State Key Laboratory of Structural Chemistry, Fujian Institute of Research on the Structure of Matter, Chinese Academy of Sciences, 155 Yangqiao Road West, Fuzhou 350002, Fujian, China. E-mails: yanxinchen; czlu@fjirsm.ac.cn

How to cite this article: Ji, M. H.; Chen, W.; She, A. S.; Yang, Y.; Shi, H. Y.; Wang, H. L.; Li, K. X.; Lin, X. M.; Chen, Y. X.; Lu, C. Z. Fluorine-doped titanium dioxide nanorod arrays for efficient photoelectrochemical water splitting. *Microstructures* **2025**, *5*, 2025072. https://dx.doi.org/10.20517/microstructures.2024.165

Received: 19 Dec 2024 **First Decision:** 4 Mar 2025 **Revised:** 22 Apr 2025 **Accepted:** 9 May 2025 **Published:** 17 Jun 2025

Academic Editors: Chunqiang Zhuang, Yongfa Zhu **Copy Editor:** Shu-Yuan Duan **Production Editor:** Shu-Yuan Duan

Abstract

TiO_2 is a well-known photocatalyst due to its excellent photocatalytic activity, low cost, and stability. However, its practical applications are limited by its poor charge transport and wide bandgap. In this study, F-doped TiO_2 nanorod arrays were synthesized using a simple chemical bath annealing method, which resulted in significantly improved properties. Among the samples, 0.05F-T (F-doped TiO_2 nanorods) exhibited the best performance, with a photocurrent of 7.34 mA/cm^2 at 1.8 V *vs.* reversible hydrogen electrode (RHE), which is 4.61 times higher than that of pure TiO_2 nanorods (1.59 mA/cm^2). Incident photon-to-current efficiency measurements showed prominent photocurrent responses in the 325-375 nm range and a slight redshift toward the visible region around 425 nm, indicating improved light absorption. The electron-hole separation efficiency was enhanced, and bandgap and flat-band potential measurements confirmed the optimization of the energy band structure. The photoelectrochemical performance for water splitting was also evaluated, with 0.05F-T achieving the highest hydrogen production of 842.28 μmol/cm^2 in 5 h at 1.8 V *vs.* RHE, which is 6.58 times higher than that of pure TiO_2 (128.05 μmol/cm^2).

These results demonstrate that F-doped TiO_2 nanorods are promising for enhancing photocatalytic hydrogen production.

Highlights

1. A simple wet chemical soaking method introduces the Fluoride (F) element into the TiO_2 lattice.

2. F element doping changes the lattice spacing of TiO_2 and optimizes the band structure.

3. The doping of the F element causes a red shift in the wavelength of TiO_2 light absorption.

4. Efficient photoelectrochemical water splitting achieved by F-doped TiO_2 nanorods.

Keywords: Photoelectrochemical water splitting, TiO_2 nanorods, photoanodes, fluoride doping

INTRODUCTION

With society's continuous development, the demand for energy has become increasingly prominent. The constant development of fossil energy and fossil fuels has led to a series of energy crises and environmental problems, such as global warming, energy crisis, and other issues that endanger human society. The key to solving such problems is finding new green energy to replace fossil energy, optimizing energy composition, and reducing carbon emissions.

As a new type of secondary energy, hydrogen energy offers several advantages, including being clean, having high energy density, and being easy to store. It is widely used in various fields and is considered a new energy source that can replace fossil energy[1]. Hydrogen (H_2) is an efficient and clean energy carrier for future sustainable energy systems[2].

At present, an environmentally friendly method is needed to obtain H_2. The main techniques for the industrial production of H_2 are electrolytic water[3] and the thermochemical method[4]. The thermochemical approach generates hydrogen through the steam reforming process of cracked petroleum and methane. Some worthless and polluting by-products, such as CO_2, NO, and other gases, can not be avoided. However, the production of H_2 from electrolytic water has problems with low energy conversion efficiency, high energy consumption, and low economy, which is not in line with the concept of green and sustainable development.

Since Fujishima and Honda[5] first used TiO_2 film for photoelectrochemical (PEC) water splitting to produce H_2 in the early 1970s, PEC water splitting has attracted extensive attention because of its environmentally friendly nature. In PEC water decomposition, a semiconductor photocatalyst converts solar energy into electrochemical energy. In other words, under sunlight, H_2 can be ideally generated by decomposing the rich water on the earth, which is an environmental and economic method. Therefore, PEC water decomposition technology is an ideal H_2 production technology. Photoelectrocatalytic decomposition of water to produce hydrogen is the most environmentally friendly and sustainable hydrogen production method[6-10].

In the past 50 years, the photocatalytic reaction on TiO_2 has aroused great interest. As a key part of photoelectrochemical cells, the semiconductor photoanode directly impacts the separation and transfer of photo-generated carriers[11]. Various modification techniques, including ion exchange, TiO_2 nanotubes (TNT) formation, and chemical bath annealing, can enhance TiO_2-based photocatalysts. Ion exchange is

commonly used to introduce dopants, improving TiO_2's electronic structure and photocatalytic performance. With its high surface area and one-dimensional nanostructure, TNT formation boosts electron transport and charge separation, enhancing photocatalytic efficiency. The chemical bath annealing method is a simple, cost-effective way to synthesize TiO_2 nanostructures, allowing for precise control over crystallinity, morphology, and doping levels, further optimizing photocatalytic properties.TiO_2 has received significant attention among various semiconductor materials due to its affordability, non-toxic nature, strong chemical stability, and eco-friendliness[12-15]. TiO_2 has an optimal band gap that supports the photocatalytic decomposition of water into hydrogen and oxygen. However, its relatively wide band gap (approximately 3.0 eV for rutile) limits its efficiency in utilizing visible light[16,17]. TiO_2 is only responsive to ultraviolet light, which accounts for 4% of the solar spectrum, which seriously limits its practical application[18,19]. Additionally, the hole diffusion path in TiO_2 is short (less than 10 ns), inhibiting charge transfer and leading to a fast recombination rate[20,21]. Currently, researchers are implementing a range of strategies, such as surface sensitization, to enhance performance[22,23], element doping[24-26] and heterostructure construction[26-30] to expand the spectral absorption range and improve the charge separation efficiency to improve the photocatalytic performance of TiO_2. Supplementary Table 1 is a comparative reference for the performance of different TiO_2 modification strategies in recent years.

In this work, the TiO_2 photoanode was modified by ion doping, and the F-doped TiO_2 nanorod array was synthesized for the photoelectrochemical water splitting to produce hydrogen. TiO_2 nanorods were grown on FTO conductive glass by the hydrothermal method, soaked in NH_4F solution before annealing, and annealed after soaking. To ensure the accuracy of the experiment, three distinct concentrations of NH_4F solution were employed: 0.01 mol/L, 0.05 mol/L, and 0.1 mol/L. The F-doped TiO_2 nanorods (F-T) prepared in three solutions were named 0.01F-T, 0.05F-T, and 0.1F-T, respectively. The TiO_2 nanorods without NH_4F solution were used as blank control samples, named TiO_2 nanorod sample (TNRS). The results showed that the electron-hole separation ability of F-doped TiO_2 nanorods was enhanced, and the photoelectrochemical performance was significantly improved. This research offers a novel perspective for designing practical photocatalysts in energy-related applications.

MATERIALS AND METHODS

Synthesis of TiO_2 nanorod arrays

The synthesis method of the TiO_2 nanorod array refers to the previously reported methods[31,32] using FTO glass as the substrate and the hydrothermal method to synthesize the TiO_2 nanorod array. Initially, the FTO glass sheet is subjected to ultrasonic cleaning using acetone (C_3H_6O, AR ≥ 99.5%, Sinopharm Chemical Reagent Co., Ltd., Shanghai, China), deionized water, and ethanol (C_2H_6O, AR ≥ 99.7%, Sinopharm Chemical Reagent Co., Ltd., Shanghai, China) for 30 min. This process eliminates oil, dust, and other contaminants from the surface, after which the sheet is dried under a nitrogen flow for later use. The volume ratio of deionized water to hydrochloric acid (37%, Sinopharm Chemical Reagent Co., Ltd., Shanghai, China) was maintained at 1:1. Subsequently, 0.6 ml of tetrabutyl titanate (TBOT, $C_{16}H_{36}O_4Ti$, AR ≥ 98.5%, Sinopharm Chemical Reagent Co., Ltd., Shanghai, China) was gradually added to the hydrochloric acid solution using a pipette gun, while stirring vigorously. After the solution is clarified, it is transferred to the reactor, and the FTO glass sheet prepared above is placed obliquely in the reactor with the conductive surface facing up. The temperature was kept at 170 °C for 6 h in a bake-out furnace, and the heating rate was 1 °C/min. After hydrothermal treatment, the glass sheet was removed and washed with ultrapure water. It can be observed that the conductive surface of the glass sheet is covered with a layer of white film. Subsequently, the glass sheet was annealed in a tubular furnace at 450 °C for 1 h under an argon atmosphere.

Synthesis method of F-doped TiO_2 nanorod array

As shown in Figure 1, it is similar to the above synthesis method. However, before annealing, it needs to soak different concentrations of NH_4F (NH_4F, AR ≥ 96.0%, Sinopharm Chemical Reagent Co., Ltd., Shanghai, China) solution, the concentrations are 0.01 mol/L, 0.05 mol/L, 0.1 mol/L respectively, and soak a piece of fresh unannealed TiO_2 in ultrapure water for comparison. The soaking time was 5 min. Then, the samples were taken out, and the residual NH_4F solution on the surface was thrown away and dried with nitrogen flow. The annealing conditions were the same as above. The samples were named according to the concentration of NH_4F soaked: TNRS (0 mol/L), 0.01F-T (0.01 mol/L), 0.05F-T (0.05 mol/L), 0.1F-T (0.1 mol/L).

PEC testing

The CHI 760E three-electrode electrochemical workstation was used to conduct photocurrent response, electrochemical impedance spectroscopy (EIS), linear sweep voltammetry (LSV), and incident photon-to-current efficiency (IPCE) tests on the samples. Supporting detailed descriptions of the information.

Materials characterization

The material was analyzed using several techniques, such as scanning electron microscopy (SEM) and X-ray diffraction (XRD). Transmission electron microscopy (TEM), high-resolution transmission electron microscopy (HRTEM), energy-dispersive X-ray spectroscopy mapping (EDS-mapping), and selected area electron diffraction (SAED) were performed on a TF20 (FEI) operating at 200 kV [TF20 (FEI) 200 kV, Thermo Fisher Scientific, Waltham, MA, USA]. The samples' atomic composition and surface state were characterized using X-ray photoelectron spectroscopy (XPS) using Al Kα rays as the excitation source.

RESULTS AND DISCUSSION

Structure and morphology

Figure 2 presents the SEM images of the material. It is clear that the FTO substrate is covered with a uniform layer of rod-shaped structures. Each rod has a cubic shape, and a neat, uneven quadrilateral structure can be observed at the top of each rod. Based on these observations, it can be inferred that the TiO_2 nanorods grow predominantly via a surface growth mechanism during their formation process [Figure 2A]. This behavior is typically observed in crystal growth, where crystals often develop into flat surfaces, straight polyhedral shapes, and other similar structures. Figure 2B-D displays the F-doped TiO_2 nanorod arrays, showing that F doping does not significantly alter the morphology of the material. The side view of the rod-shaped material is shown in Supplementary Figure 1, revealing that the length of the rods ranges from 3.0 μm to 4.0 μm, with a diameter of approximately 100 nm to 300 nm. Each nanorod is independent and perpendicular to the substrate, with no noticeable impurities observed.

Figure 3A shows the XRD spectra of the TiO_2 nanorod array and F-doped TiO_2 nanorod array, from which we can see that there are mainly two components. Among them, there are apparent characteristic peaks at 26.62°, 33.8°, 37.86°, 51.62°, 61.66°, and 65.56° corresponding to the characteristic peak of SnO_2, which is the characteristic peak of FTO glass substrate. In addition, there are peaks at 36.26°, 41.4°, 54.48°, and 62.96° corresponding to the rutile phase of TiO_2, and the corresponding crystal planes are (101), (111), (211), and (002). No peak proves that the synthesized TiO_2 material is pure rutile phase TiO_2, rather than the mixed phase of anatase and rutile phase. Figure 3B is a partial enlarged view of Figure 3A. It can be seen that the peak of F-doped TiO_2 shifts to the right as a whole. This is because after F-doping, F^- will replace part of O^{2-}, resulting in crystal face contraction and smaller crystal face spacing. However, with the increase of doping amount, the peak will gradually shift to the right, which shows that the change of doping amount will make more f- enter the lattice of TiO_2, resulting in lattice distortion. We tested EDS mapping maps based on SEM. Supplementary Figure 2 shows that O, Ti, and F elements are uniformly distributed, with a relatively low

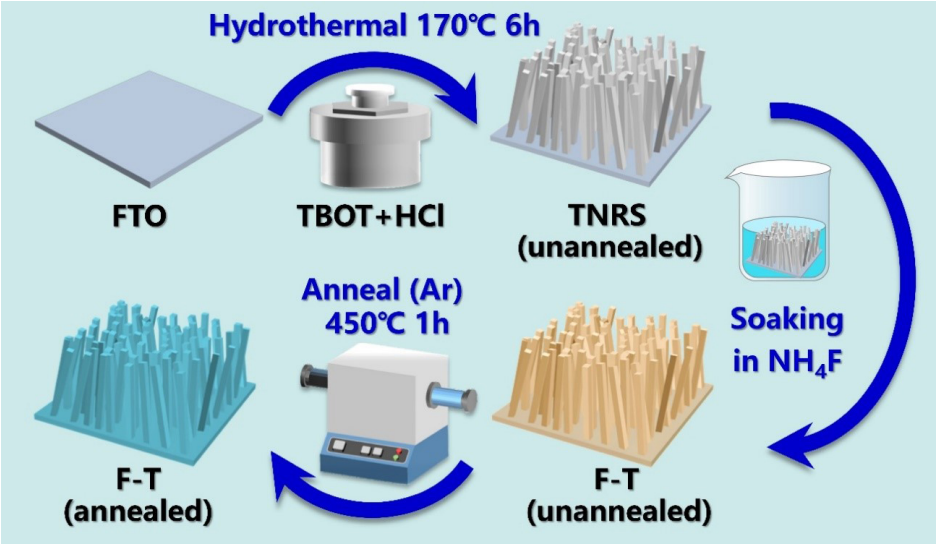

Figure 1. The typical preparation process of the F-T photoanode. TBOT: Tetrabutyl titanate; TNRS: TiO_2 nanorod sample; FTO: flourine-doped tin oxide; F-T: F-doped TiO_2 nanorods.

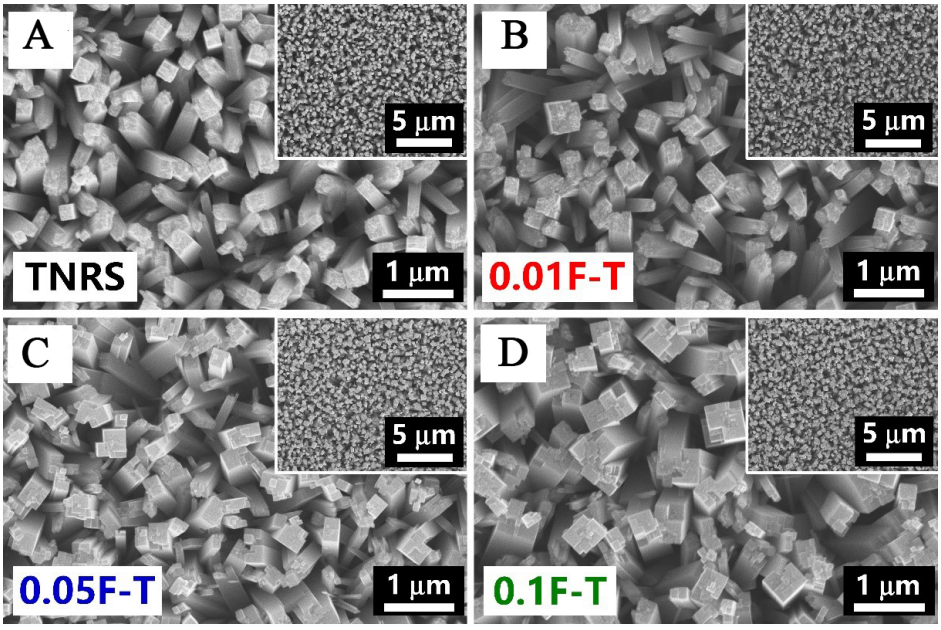

Figure 2. SEM images of (A) pristine TNRS photoanode; (B) 0.01F-T photoanode; (C) 0.05F-T photoanode; and (D) 0.1F-T. SEM: Scanning electron microscopy; TNRS: TiO_2 nanorod sample; F-T: F-doped TiO_2 nanorods.

content of the F element, proving the successful loading of the F element on TiO_2 nanorods.

To further study the microstructure of the prepared titanium dioxide samples, we carried out HRTEM measurements, as shown in Figure 4. Figure 4A is the HRTEM diagram of the TNRs sample. It can be seen from the diagram that this sample has clear lattice stripes. After measurement, the result is that the lattice spacing of TiO_2 is 0.321nm, and the corresponding crystal plane is (110). From the illustration in Figure 4A, it can also be seen that the distance between the two peaks is 0.321nm. The crystal planes (1-1-1), (110), and (1-10) can be found from the SAED spectra. Figure 4B is the HRTEM diagram of the 0.05F-T sample. Based

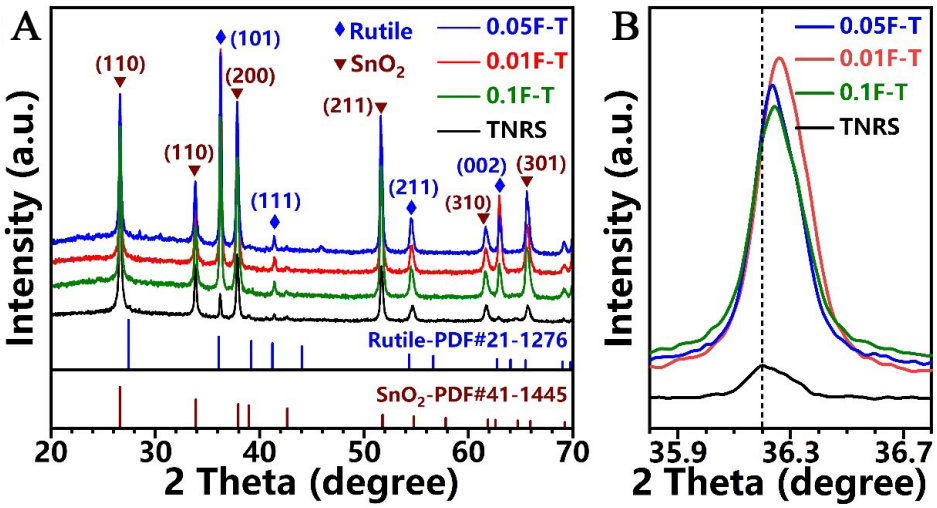

Figure 3. XRD patterns of TNRS photoanode, 0.01F-T photoanode, 0.05F-T photoanode, 0.1F-T photoanode (A); and 35.8°-36.8° refined spectrum (B). XRD: X-ray diffraction; TNRS: TiO_2 nanorod sample; F-T: F-doped TiO_2 nanorods.

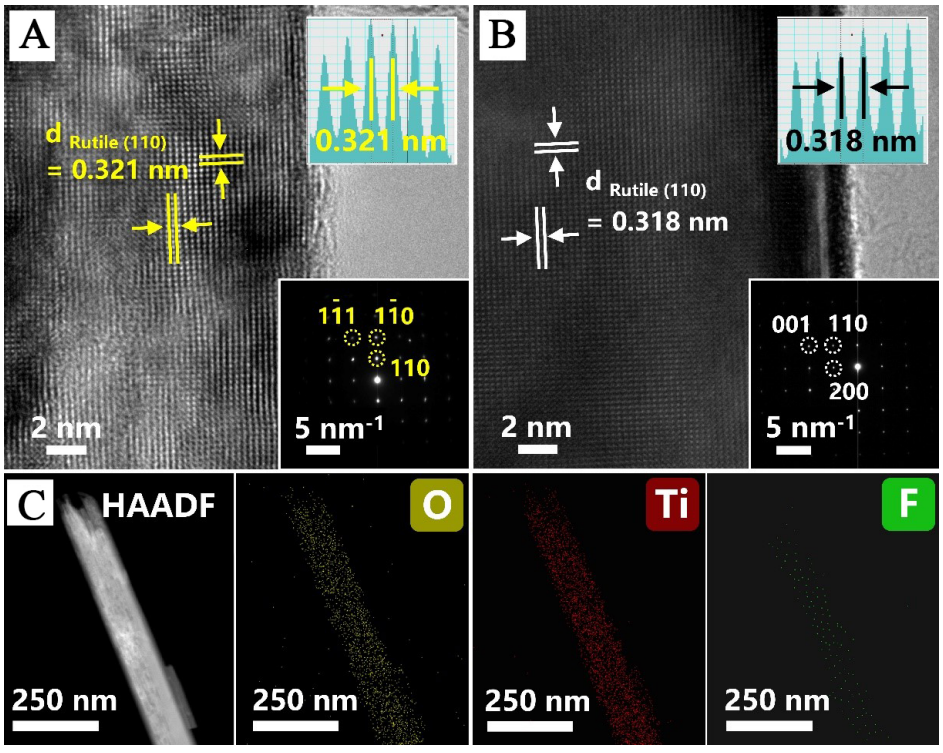

Figure 4. HRTEM patterns of TNRS photoanode (A); 0.05F-T photoanode (B); inset is SAED, and EDS Mapping maps of 0.05F-T photoanode (C). HRTEM: high-resolution transmission electron microscopy; F-T: F-doped TiO_2 nanorods; TNRS: TiO_2 nanorod sample; SAED: selected area electron diffraction; EDS-mapping: energy-dispersive X-ray spectroscopy mapping.

on the diagram, the measured lattice spacing is 0.318 nm. Additionally, as shown in Figure 4B, the distance between the two peaks is also 0.318 nm. After F ion doping, the lattice spacing decreased slightly. The crystal planes (111), (110), and (001) can be found from the SAED spectra. The EDS mapping of the 0.05F-T photoanode is illustrated in Figure 4C. The elements O, Ti, and F are uniformly distributed within the nanorods. Although the concentration of F is relatively low, it remains detectable.

Figure 5 shows the XPS test result of the material. The standard peak of carbon used in the test data is 284.8 eV, which is used to correct the corresponding spectrum. Figure 5A is the total spectrum of four samples. It can be seen that the carbon element has a standard peak of 284.8 eV. In addition, the Ti and O element peaks can be seen. Because the doping amount of the F element is minimal, no peak signal of the F element is observed in the total spectrum. Figure 5B is the spectrum of the oxygen element. A double-peak structure is visible. The peak near 530 eV represents the peak of lattice oxygen, and the peak near 532.2 eV represents the peak of surface-adsorbed oxygen. Figure 5C is the XPS spectrum of element F. We can see that at 685 eV, with the increase of the concentration of element F, a peak gradually appears in the spectra of 0.05F-T and 0.1F-T. Therefore, it can be judged that fluorine exists in the form of F^-. However, it is not observed in TNRS and 0.01F-T. It is considered that the amount of the F element is too small, and the signal is not apparent. Figure 5D shows the peak position of Ti 2p. You can see the bimodal signals of standard TiO_2, which are 458.5 eV and 464.2 eV, respectively, and the energy difference between the two peaks is 5.7 eV, indicating that titanium exists in the form of Ti^{4+}[33]; compared with pure titanium rod, the titanium element peak of F-doped sample moves slightly to the direction of higher binding energy, indicating that F replaces part of O, and the electrostatic attraction to titanium increases, resulting in the shift of peak position.

Photoelectrochemical performance

Figure 6A shows the LSV curves of the four samples. It can be seen that the F-doped TiO_2 shows excellent optical response and photocurrent density, which are far greater than those of pure TiO_2 nanorods. The photocurrent density of 0.05F-T is the largest. Under the bias voltage of 1.8 V *vs.* reversible hydrogen electrode (RHE), the photocurrent density reaches 7.34 mA/cm^2, which is 4.61 times that of TNRS (1.59 mA/cm^2). The photocurrent density of 0.01F-T and 0.1F-T was 5.31 mA/cm^2 and 5.18 mA/cm^2, respectively, which were 3.33 and 3.25 times that of TNRS, showing excellent photocatalytic performance. At the bias voltage of 1.23 V *vs.* RHE, the corresponding photocurrent densities are TNRS: 1.56 mA/cm^2, 0.01F-T: 5.06 mA/cm^2, 0.05F-T: 6.99 mA/cm^2, 0.1F-T: 4.80 mA/cm^2. We can see that all materials showed a little increase in performance under medium to high bias voltages, indicating that the material can achieve higher photocurrent density under low bias voltages. This conclusion can also be drawn from applied bias photo-to-current efficiency (ABPE), where the sample reaches its maximum value at 0.63 V *vs.* RHE. To further explore the method of doping F ions on TiO_2 nanorods, we changed the doping method of F ions. Unlike the previous modification method, the annealed TiO_2 nanorods were immersed in an NH_4F solution and annealed again. Supplementary Figure 3 shows that the photocurrent density of the modified 0.05-F-T-2 sample did not increase, indicating that successful doping of F ions requires doping before TiO_2 crystallization. At the same time, a comparative experiment with or without a hole trap agent was also done in Supplementary Figure 4, and the photocurrent density increased after the electrolyte was replaced with 0.1 M Na_2SO_3.

Figure 6B is the ABPE curve calculated according to the photocurrent density. It can be seen that the maximum values of all samples are reached at 0.63 V *vs.* RHE, which are TNRS: 2.11%, 0.01F-T: 6.09%, 0.05F-T: 9.38%, 0.1F-T: 6.03%, respectively. The I-t curve was analyzed to demonstrate the material's stability, as presented in Figure 6C. The sample can also maintain excellent stability under high voltage. After 1 h of testing, the photoelectric catalytic performance of the material has not significantly decreased, indicating the photo corrosion resistance and excellent stability of the material. Supplementary Figure 5 shows the photocurrent curve of long illumination at 12 h. A photoelectric hydrogen production test was conducted to evaluate the hydrogen production performance of the material by applying a bias voltage. The optoelectronic hydrogen production test was conducted under the bias voltage of 1.8 V *vs.* RHE and under the condition of 3.5 times that of AM 1.5 G for 5 h. It can be seen from Figure 6D that the hydrogen production of the F-doped sample is much higher than that of its undoped pure TiO_2 nanorod array, showing excellent photocatalytic water decomposition performance. The hydrogen production of each

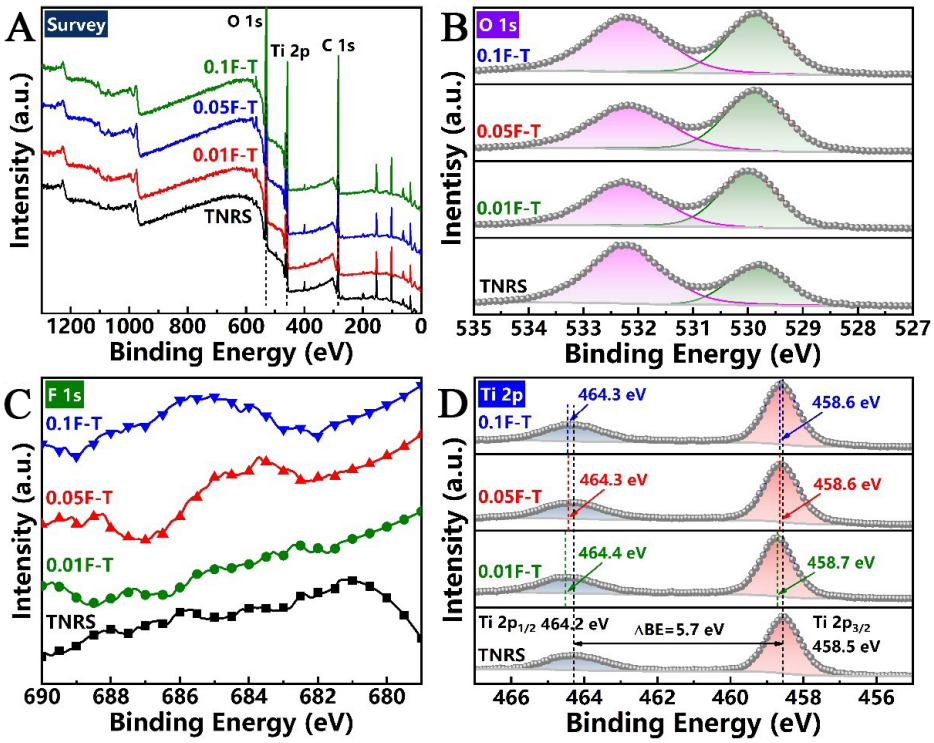

Figure 5. (A) XPS full spectra of photoanode; (B) XPS spectra of O 1s; (C) F 1s; and (D) Ti 2p. XPS: X-ray photoelectron spectroscopy.

sample is as follows: TNRS: 128.05 μmol/cm^2, 0.01F-T: 582.53 μmol/cm^2, 0.05F-T: 842.28 μmol/cm^2, 0.1F-T: 572.99 μmol/cm^2. As shown in Figure 6E, after F doping, the starting potential of the photoanode undergoes a significant negative shift with increasing doping levels. The starting potential of pure TiO_2 is 0.159 V *vs.* RHE, while for 0.01F-T, it is 0.100 V *vs.* RHE, for 0.05F-T, it is 0.030 V *vs.* RHE, and for 0.1F-T, it is 0.013 V *vs.* RHE. This indicates that F doping significantly lowers the starting potential of the photoanode, and the negative shift becomes more pronounced with higher doping concentrations. The addition of F likely improves the electronic structure and energy band alignment of TiO_2, enhancing the water oxidation kinetics, reducing the overpotential, and thereby improving the overall photoelectrochemical performance of TiO_2.

We calculated the hole transfer efficiency between the electrode and the electrolyte to better illustrate the separation of charge carriers. The surface efficiency ($\eta_{surface}$) is determined using the following equation[34-36]:

$$\eta_{surface} = J_{H_2O}/J_{Na_2SO_3}$$

In this formula, J_{H_2O} is the LSV test of the photoanode in 1 M KOH electrolyte, and $J_{Na_2SO_3}$ is the LSV test of the photoanode in 1 M KOH + 1 M Na_2SO_3 electrolyte. Adding Na_2SO_3 facilitates rapid oxidation kinetics due to the low activation energy of SO_3^{2-}. This ensures that all photo-generated holes reaching the interface between the photoelectric electrode and the electrolyte are immediately consumed, allowing surface charge recombination to be neglected. Thus, Na_2SO_3 functions effectively as a hole scavenger.

As shown in Figure 6F, the incorporation of fluoride (F) into the TiO_2 photoanode significantly improves the hole transfer efficiency between the photoanode and the electrolyte. At a bias voltage of 1.23 V *vs.* RHE, the surface efficiency ($\eta_{surface}$) of the pure TNRS is 84%. In contrast, the F-doped samples exhibit a

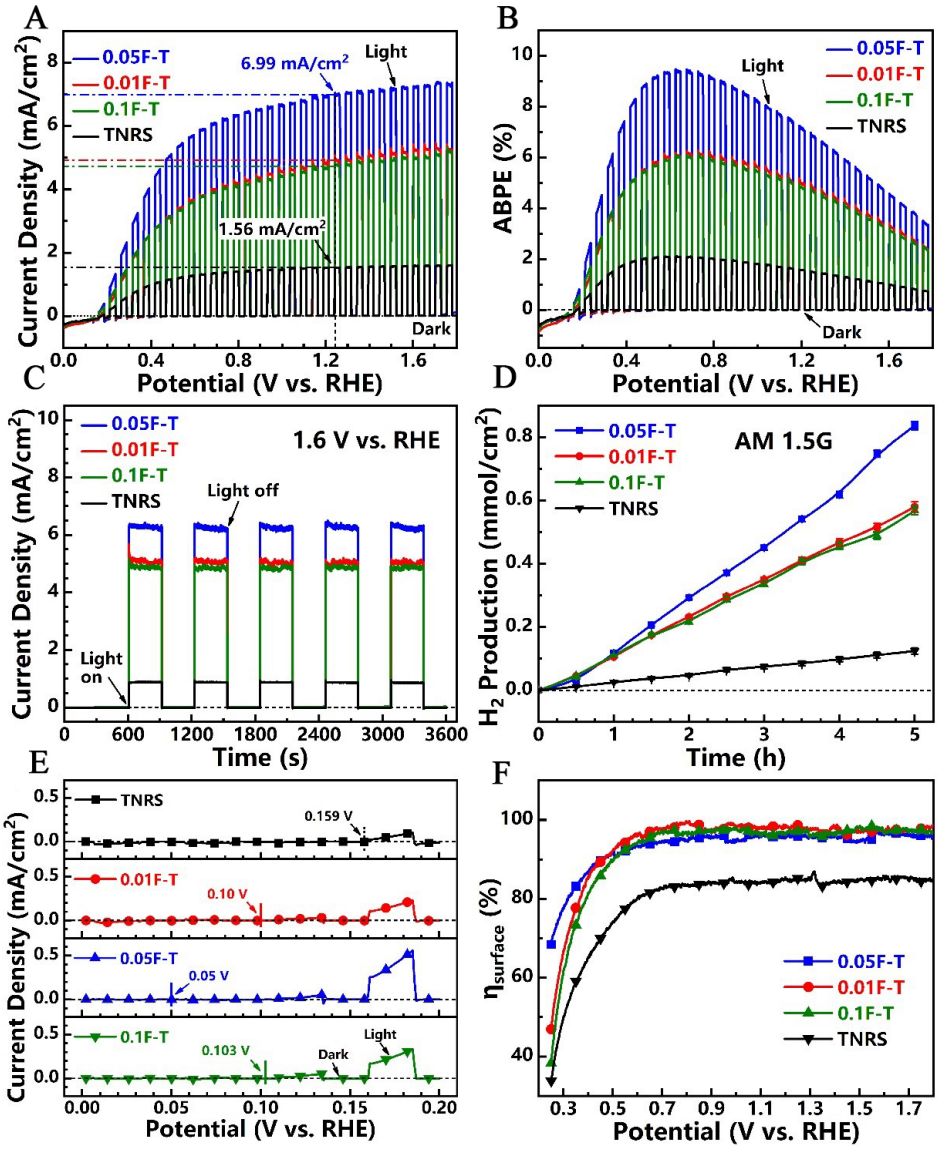

Figure 6. LSV curves for TNRS photoanode, 0.01F-T photoanode, 0.05F-T photoanode, and 0.1F-T photoanode under a light power of 100 mW (A); ABPE curves for TNRS, 0.01F-T, 0.05F-T, and 0.1F-T photoanode (B); I-t curves for TNRS, 0.01F-T, 0.05F-T, and 0.1F-T photoanode (C); hydrogen production capacity tests for TNRS, 0.01F-T, 0.05F-T, and 0.1F-T photoanode under 3.5 times AM 1.5 G simulated sunlight (D); initial potential tests for TNRS, 0.01F-T, 0.05F-T, and 0.1F-T photoanode (E); $\eta_{surface}$ curves for TNRS, 0.01F-T, 0.05F-T, and 0.1F-T photoanode (F). RHE: reversible hydrogen electrode; LSV: Linear sweep voltammetry; TNRS: TiO_2 nanorod sample; F-T: F-doped TiO_2 nanorods; ABPE: applied bias photo-to-current efficiency; AM: air mass.

remarkable enhancement in this efficiency, reaching approximately 95%. This improvement suggests that the doping of TiO_2 with fluoride not only increases the hole transfer efficiency but also helps to reduce the recombination of photo-generated electron-hole pairs. The enhanced hole transfer efficiency between the photoanode and the electrolyte is crucial in improving the overall photoelectrochemical performance, as it facilitates more effective charge separation and transport during the water-splitting reaction.

Figure 7A-H displays the wavelength-dependent photocurrent density curves. It can be observed that as the bias voltage increases, the photocurrent density and IPCE of the material also increase. Figure 7A and B shows that, compared to the TNRS sample, the F-doped samples exhibit superior photocurrent density and

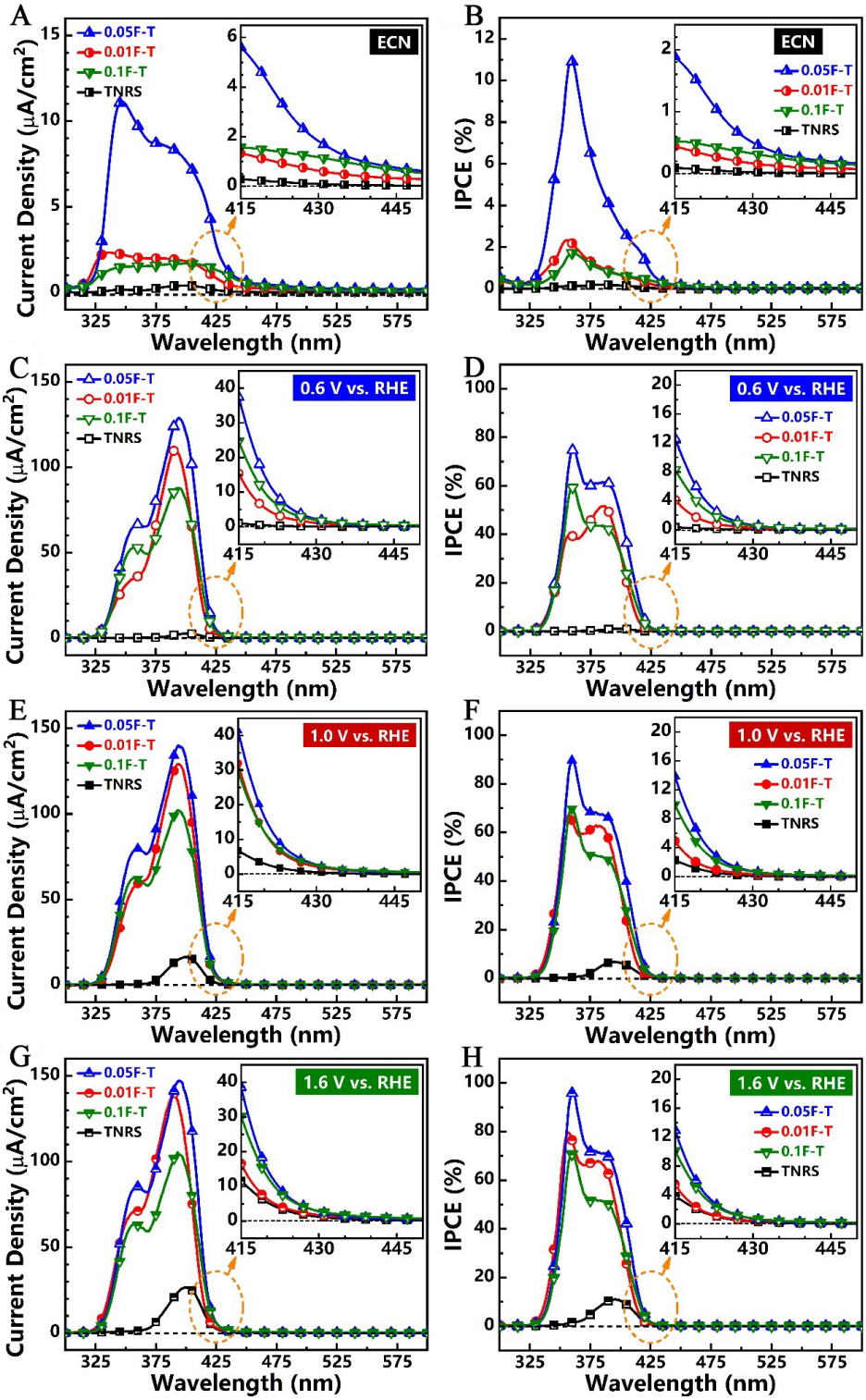

Figure 7. Wavelength scanning *vs.* photocurrent density curves and wavelength scanning *vs.* IPCE curves of TNRS, 0.01F-T, 0.05F-T, and 0.1F-T photoanode in Electrochemical noise model (A and B); the wavelength scanning *vs.* photocurrent density /IPCE curves with bios voltage at 0.6 V (*vs.* RHE) (C and D); at 1.0 V *vs.* RHE (E and F); and 1.6 V *vs.* RHE (G and H) of TNRS, 0.01F-T, 0.05F-T, and 0.1F-T photoanodes, respectively. 1 M KOH as electrolyte. ECN: Electrochemical noise; RHE: reversible hydrogen electrode; IPCE: incident photon-to-current efficiency; F-T: F-doped TiO_2 nanorods; TNRS: TiO_2 nanorod sample.

IPCE in the wavelength range of 325-375 nm. This indicates that F doping enhances the UV absorption range of the material. In Figure 7C-H, it can be seen that the performance of 0.05F-T is the best. Figure 7G shows that 0.05F-T reaches the maximum photocurrent density of 147.24 μA/cm^2 at 388 nm, with the corresponding maximum IPCE value of 98.1% at 355 nm. The photocurrent density of TNRS peaks at 395 nm, with a performance of 21.49 μA/cm^2, and the IPCE peaks at 393 nm, reaching 13.8%. 0.01T-F has a maximum photocurrent density of 102.22 μA/cm^2 at 392 nm, while the IPCE reaches a peak value of 74.6% at 356 nm. 0.1F-T reaches its maximum photocurrent density of 138.80 μA/cm^2 at 384 nm, and the IPCE peaks at 79.0% at 356 nm. Additionally, it can be observed that for the F-doped samples, there is a slight red shift in the photocurrent cutoff wavelength at 425 nm, suggesting that F doping reduces the bandgap of the titanium dioxide material and expands its optical response range.

Figure 8A shows the band gap of the material calculated based on IPCE. The figure indicates that the band gap of pure TiO_2 is 2.96 eV, which is close to the theoretical band gap value of 3.0 eV for rutile-phase TiO_2. Furthermore, the band gap of F-doped samples is lower than that of the undoped materials, measuring 2.931 eV for 0.01F-T, 2.917 eV for 0.05F-T, and 2.932 eV for 0.1F-T.

The electrochemical impedance spectroscopy (EIS) results are shown in Figure 8B. The EIS curve of the sample shows a standard semicircle, and the resistance value of the F-doped sample is significantly lower than that of the undoped pure titanium rod TNRS, indicating that F-doping improves the electron transfer efficiency of TiO_2 and reduces the resistance value of the sample. This can be validated by fitting the Nyquist plot using an equivalent circuit model and by comparing the results obtained from the EIS measurements. As shown in Supplementary Table 2, Rct represents the charge transfer resistance between the photoanode and electrolyte. The Rct value of 0.05F-T is 55.2 kΩ, significantly lower than the Rct value of TNRS (169.0 kΩ). Additionally, all curves in the Nyquist plot intersect at the origin of the coordinate axis, suggesting that the resistance of the solution can be considered negligible.

Determine the flat band potential of these samples through Mott-Schottky measurement, as shown in Figure 8C. The Mott-Schottky equation can be used to fit the flat band potentials of TNRS, 0.01F-T, 0.05F-T, and 0.1F-T, which are -0.14 V *vs.* RHE, -0.28 V *vs.* RHE, -0.32 V *vs.* RHE, and -0.38 V *vs.* RHE, respectively. Compared to the undoped sample, the flat band potential of the F-doped titanium oxide nanorod array is more negative, indicating that its photo-generated electrons have stronger reduction ability and are more conducive to the photocatalytic hydrogen evolution reaction.

As shown in Figure 9A-D, based on DFT calculations, the electronic band structure and density of states of the sample were obtained. As shown in Figure 9A, since the conduction band (CB) minimum and valence band (VB) maximum are located at the Γ point, TiO_2 is considered a direct semiconductor with a band gap width of 2.457 eV. This configuration enhances the potential for ion doping in materials featuring broader band gaps. The band gap width of F-T is 0.908 eV, as shown in Figure 9B. Figure 9C's total and partial density of states detail the band structure and composition of the CB and VB, highlighting the significant impact of F doping on TiO_2's photoelectronic properties[37]. Figure 9D demonstrates that hybridization between F 1s and Ti 3d orbitals significantly narrows the band gap in TiO_2 and enhances electronic delocalization. This promotes electron transport, thereby facilitating the hydrogen evolution process.

Based on the fundamental structure of TiO_2 [Figure 10A and B], the calculated electron localization function (ELF) diagram explains the local electron distribution compared to pure TiO_2 [Figure 10C]. Figure 10A and B shows the crystalline structure of pure TiO_2, where Ti and O atoms are arranged in a regular lattice configuration. Figure 10D and E displays the structure of TiO_2 doped with F (F-T). The

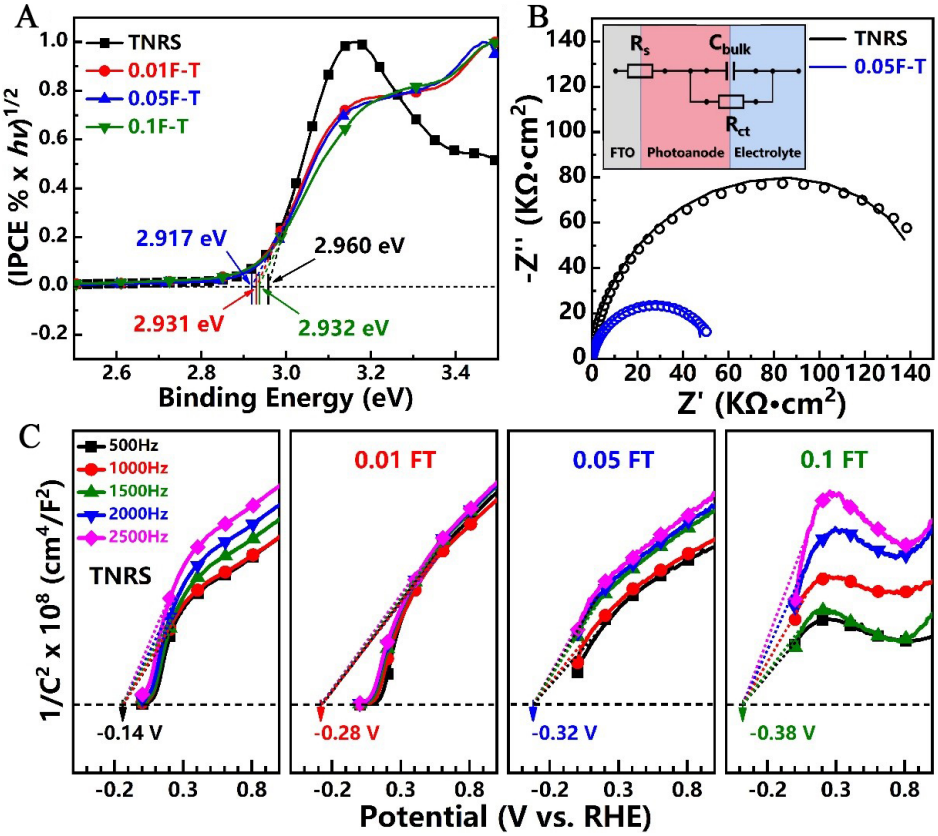

Figure 8. (A) Band gap of TNRS, 0.01F-T, 0.05F-T, and 0.1F-T photoanode; (B) EIS patterns of TNRS photoanode, 0.01F-T photoanode, 0.05F-T photoanode, and 0.1F-T photoanode; (C) M-S patterns (0.1 M Na_2SO_4 as electrolyte, Ag/AgCl as reference electrode, convert the potential into RHE potential) of TNRS, 0.01F-T0.05F-T, and 0.1F-T photoanode. TNRS: TiO_2 nanorod sample; F-T: F-doped TiO_2 nanorods; RHE: reversible hydrogen electrode; EIS: electrochemical impedance spectroscopy.

introduction of F has noticeably altered the local lattice structure of TiO_2. By comparing the ELF in Figure 10C and 10F, it is evident that the electron localization distribution in TiO_2 changes after F doping[38], particularly around the In atoms, where the degree of electron localization differs. This suggests that F doping may influence the material's electronic structure and charge transport properties, enhancing its photocatalytic performance.

Photoelectrochemical mechanism for water splitting under solar light

Based on the obtained flat band potential and the electrochemical band gap, which is shown and discussed in Figure 8, the conduction band position of the material can be calculated, thereby obtaining the energy band structure of the material, as shown in Figure 11. The graph shows that the band range of TNRS is -0.14 eV to 2.82 eV, with a band gap of 2.96 eV. After doping with the F element, the band range of the 0.05F-T sample is -0.32 eV to 2.59 eV, with a reduced band gap of 2.91 eV. A smaller band gap improves the material's light absorption ability.

Based on the above discussion, we further analyzed the mechanism of F-doped TiO_2 in photoelectrochemical water splitting. Under sunlight irradiation, the TiO_2 photoanode generates photo-generated electron-hole pairs. The photo-generated holes react with water molecules on the photoanode surface to produce oxygen. In contrast, the photo-generated electrons are transferred to the photocathode through an external bias voltage and react with water to produce hydrogen gas. For the original TNRS

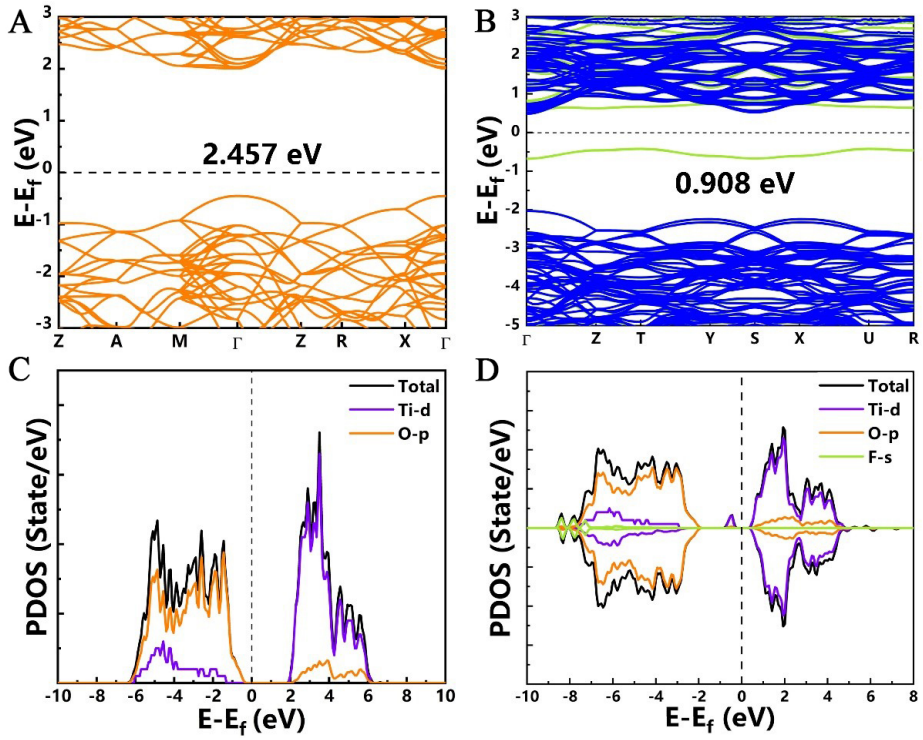

Figure 9. Electronic structure properties. (A) Bandwidth of TiO_2; (B) Bandwidth of F-T sample; (C) Total density of states and partial density of states of TiO_2; (D) Total density of states and partial density of states of F-T sample. F-T: F-doped TiO_2 nanorods.

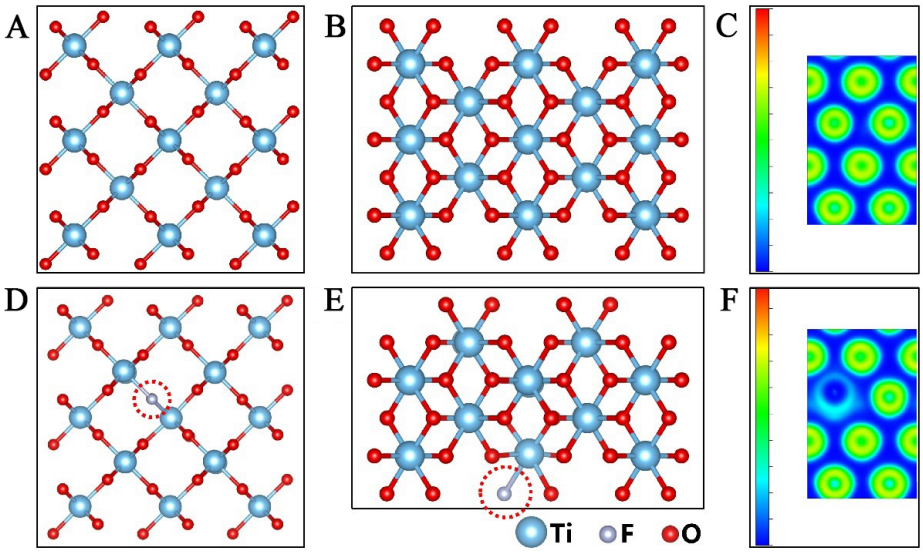

Figure 10. Schematic structures of (A and B) TiO_2 and (D and E) F-T; (C) ELF map of TiO_2 and (F) F-T. F-T: F-doped TiO_2 nanorods; ELF: electron localization function.

sample, TiO_2 has a wide bandgap and weak sunlight absorption ability, resulting in limited photocatalytic performance. However, after introducing fluorine, the TiO_2 lattice changes, and the bandgap is significantly reduced, leading to a notable increase in the material's ability to absorb visible light. The F-doped TiO_2 material can more effectively absorb visible light and utilize photo-generated electrons, significantly

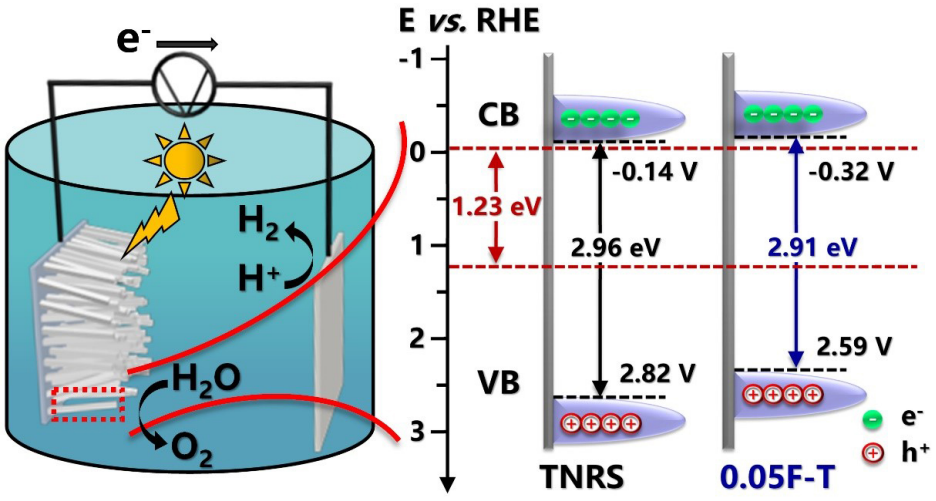

Figure 11. Schematic diagram of energy band structure. TNRS: TiO_2 nanorod sample; CB: conduction band; VB: minimum and valence band; RHE: reversible hydrogen electrode.

improving its photocatalytic performance. Furthermore, we found that F-doping significantly enhances the hole transfer efficiency in the photoanode, while reducing the recombination of photo-generated electrons and holes. The charge transfer resistance of the F-doped samples is significantly reduced, resulting in an overall increase in photocurrent density. This improved hole transfer efficiency and reduced charge transfer resistance facilitate the efficient photoelectrochemical water splitting process. Through these optimizations, F-doped TiO_2 demonstrates higher photocatalytic stability and stronger photoelectrochemical performance, especially in applying photocatalytic water splitting[39].

CONCLUSION

In summary, F-doped TiO_2 nanorod arrays were synthesized for photocatalytic decomposition of water to produce hydrogen. We characterized the physical structure and microstructure of the material through XRD, SEM, HRTEM, and other tests, and the results showed that TiO_2 nanorods were successfully synthesized. In addition, through XRD, XPS, and EDS mapping, we determined that F was successfully doped into the material's lattice. We have demonstrated through a series of photoelectrochemical tests that F-doped TiO_2 has been optimized in photoelectrochemical properties compared to pure TiO_2. At the same time, $\eta_{surface}$ testing has shown that the electron-hole separation ability of titanium dioxide nanorods is enhanced after F doping, achieving high photoelectrochemical properties. In the photocatalytic performance test, 0.05F-T showed excellent performance. At a bias voltage of 1.23 V *vs.* RHE, the photocurrent density of 0.05F-T reaches 6.99 mA/cm^2, while the performance of TNRS is 1.56 mA/cm^2, 4.48 times that of TNRS. The I-t curves demonstrate that all materials possess good stability.

In the wavelength scanning photocurrent density test, we observed that the light absorption ability of TNRS was cut off at around 425 nm, while the sample doped with F showed a redshift, indicating that the light absorption ability of the sample doped with F was improved. The bandgap width of the material was calculated through IPCE, and the Mott-Schottky test characterized the position of the flat band potential. The results calculated based on this indicate that the energy band structure of the material has been optimized. In addition, electrochemical impedance testing and fitting results indicate decreased charge transfer resistance between the photoanode and electrolyte. Finally, the photoelectrochemical performance of the material for water splitting to produce hydrogen was tested. Among these, 0.05F-T had the best performance, achieving a hydrogen production rate of 842.28 μmol/cm^2 under a bias voltage of 1.8 V *vs.*

RHE, 5 h, and 3.5 times AM 1.5 G light, which was 6.58 times TNRS, and its performance was 128.05 μmol/cm^2.

DECLARATIONS

Authors' contributions

Conceptualization: Chen, Y. X.; Lu, C. Z.
Methodology: Ji, M. H.; Chen, W.
Investigation: She, A. S.
Validation: Shi, H. Y.
Formal analysis: Yang, Y.; Wang, H. L.
Data curation: Li, K. X.; Lin, X. M.
Writing - original draft preparation: Ji, M. H.; Chen, W.
Writing, reviewing, and editing: Chen, Y. X.; Lu, C. Z.
Supervision: Chen, Y. X.; Lu, C. Z.
Project administration: Chen, Y. X.; Lu, C. Z.
Funding acquisition: Chen, Y. X.; Lu, C. Z.
All authors have read and agreed to the published version of the manuscript.

Availability of data and materials

Some results supporting the study are presented in the Supplementary Materials. Other raw data that support the findings of this study are available from the corresponding author upon reasonable request.

Financial support and sponsorship

This work was supported by the Natural Science Foundation of Fujian Province, China (No. 2023H0046), the XMIREM autonomously deployment project, China (No. 2023CX10, No. 2023GG01), and the National Natural Science Foundation of China (No. 22272069 and No. 22472074).

Conflicts of interest

All authors declared that there are no conflicts of interest.

Content of Ethical approval and consent to participate

Not applicable.

Consent for publication

Not applicable.

REFERENCES

1. Scheffe, J. R.; Haussener, S.; Patzke, G. R. Solar hydrogen production. *Energy. Tech.* **2022**, *10*, 2101021. DOI
2. Zou, Z.; Ye, J.; Sayama, K.; Arakawa, H. Direct splitting of water under visible light irradiation with an oxide semiconductor photocatalyst. *Nature* **2001**, *414*, 625-7. DOI PubMed
3. Voloshchenko, G. N. Production of hydrogen through high-temperature electrolysis of water. *Nanotechnol. Russia.* **2020**, *15*, 333-40. DOI
4. Cai, L.; He, T.; Xiang, Y.; Guan, Y. Study on the reaction pathways of steam methane reforming for H_2 production. *Energy* **2020**, *207*, 118296. DOI
5. Fujishima, A.; Honda, K. Electrochemical photolysis of water at a semiconductor electrode. *Nature* **1972**, *238*, 37-8. DOI
6. Ding, C.; Shi, J.; Wang, Z.; Li, C. Photoelectrocatalytic water splitting: significance of cocatalysts, electrolyte, and interfaces. *ACS. Catal.* **2017**, *7*, 675-88. DOI

7. Cho, I. S.; Logar, M.; Lee, C. H.; Cai, L.; Prinz, F. B.; Zheng, X. Rapid and controllable flame reduction of TiO_2 nanowires for enhanced solar water-splitting. *Nano. Lett.* **2014**, *14*, 24-31. DOI PubMed
8. Tong, M.; Wang, T.; Lin, S.; et al. Ultra-thin carbon doped TiO_2 nanotube arrays for enhanced visible-light photoelectrochemical water splitting. *Appl. Surf. Sci.* **2023**, *623*, 156980. DOI
9. Shi, H.; Chen, Y.; Ji, M.; et al. A novel structure Ti/Fe_2O_3/Cu_2S/$Co(OH)_x$ enhances the photoelectrochemical water splitting performance of iron oxide. *Chem. Synth.* **2024**, *4*, 45. DOI
10. Tan, C.; Cao, X.; Wu, X. J.; et al. Recent advances in ultrathin two-dimensional nanomaterials. *Chem. Rev.* **2017**, *117*, 6225-331. DOI
11. Qiu, Y.; Pan, Z.; Chen, H.; et al. Current progress in developing metal oxide nanoarrays-based photoanodes for photoelectrochemical water splitting. *Sci. Bull. (Beijing).* **2019**, *64*, 1348-80. DOI
12. Lianos, P. Review of recent trends in photoelectrocatalytic conversion of solar energy to electricity and hydrogen. *Appl. Catal. B-Environ.* **2017**, *210*, 235-54. DOI
13. Kment, S.; Riboni, F.; Pausova, S.; et al. Photoanodes based on TiO_2 and α-Fe_2O_3 for solar water splitting - superior role of 1D nanoarchitectures and of combined heterostructures. *Chem. Soc. Rev.* **2017**, *46*, 3716-69. DOI
14. Jabbar, Z. H.; Graimed, B. H.; Ammar, S. H.; et al. The latest progress in the design and application of semiconductor photocatalysis systems for degradation of environmental pollutants in wastewater: Mechanism insight and theoretical calculations. *Mater. Sci. Semicond. Process.* **2024**, *173*, 108153. DOI
15. Wang, Y.; Huang, Y.; Ho, W.; Zhang, L.; Zou, Z.; Lee, S. Biomolecule-controlled hydrothermal synthesis of C-N-S-tridoped TiO_2 nanocrystalline photocatalysts for NO removal under simulated solar light irradiation. *J. Hazard. Mater.* **2009**, *169*, 77-87. DOI PubMed
16. Vorontsov, A. V.; Smirniotis, P. G. Structure, electronic and optical properties of bilayer anatase nanoribbons. *Comput. Mater. Sci.* **2018**, *155*, 266-81. DOI
17. Meena, B.; Subramanyam, P.; Suryakala, D.; Biju, V.; Subrahmanyam, C. Efficient solar water splitting using a CdS quantum dot decorated TiO_2/Ag_2Se photoanode. *Int. J. Hydrog. Energy.* **2021**, *46*, 34079-88. DOI
18. Kaushal, N.; Taha, A. A.; Tyagi, S.; Smirniotis, P. G. NH_2-MIL-101(Fe)/N-CNDs as a visible light photocatalyst for degradation of fluoroquinolone antibiotics in water. *Mater. Chem. Phys.* **2025**, *332*, 130198. DOI
19. Amal, R.; Belver, C.; Wang, Y. Enriched horizon of applied catalysis b: environment and energy. *Appl. Catal. B-. Environ.* **2024**, *343*, 123593. DOI
20. Han, C.; Yan, L.; Zhao, W.; Liu, Z. TiO_2/CeO_2 core/shell heterojunction nanoarrays for highly efficient photoelectrochemical water splitting. *Int. J. Hydrog. Energy.* **2017**, *42*, 12276-83. DOI
21. Guo, Q.; Zhou, C.; Ma, Z.; Yang, X. Fundamentals of TiO_2 photocatalysis: concepts, mechanisms, and challenges. *Adv. Mater.* **2019**, *31*, e1901997. DOI
22. Abdelkarim, O.; Mirzaei, A.; Selopal, G. S.; et al. Constructing quantum dots sensitized TiO_2 nanotube p-n heterojunction for photoelectrochemical hydrogen generation. *Chem. Eng. J.* **2022**, *446*, 137312. DOI
23. Sharma, D.; Mehta, B. Nanostructured TiO_2 thin films sensitized by CeO_2 as an inexpensive photoanode for enhanced photoactivity of water oxidation. *J. Alloys. Compd.* **2018**, *749*, 329-35. DOI
24. Yadav, S.; Jaiswar, G. Review on undoped/doped TiO_2 nanomaterial; synthesis and photocatalytic and antimicrobial activity: review on undoped/doped TiO_2 nanomaterial. *J. Chin. Chem. Soc.* **2017**, *64*, 103-16. DOI
25. Huang, J.; Dou, L.; Li, J.; Zhong, J.; Li, M.; Wang, T. Excellent visible light responsive photocatalytic behavior of N-doped TiO_2 toward decontamination of organic pollutants. *J. Hazard. Mater.* **2021**, *403*, 123857. DOI
26. Dey, S.; Roy, S. C. Influence of Ce doping on morphology, crystallinity and photoelectrochemical charge transfer characteristics of TiO_2 nanorod arrays grown on conductive glass substrate. *J. Alloys. Compd.* **2021**, *881*, 160481. DOI
27. Jiang, X.; Che; YX; Lu, C. Z. Bio-inspired materials for photocatalytic hydrogen production. *Chin. J. Struct. Chem.* **2020**, *39*, 2123-30. DOI
28. Jiang, H.; Li, M.; Liu, J.; Li, X.; Tian, L.; Chen, P. Alkali-free synthesis of a novel heterostructured CeO_2-TiO_2 nanocomposite with high performance to reduce Cr(VI) under visible light. *Ceram. Int.* **2018**, *44*, 2709-17. DOI
29. Lu, H.; Fang, S.; Hu, J.; et al. Fabrication of a TiO_2/Fe_2O_3 core/shell nanostructure by pulse laser deposition toward stable and visible light photoelectrochemical water splitting. *ACS. Omega.* **2020**, *5*, 19861-7. DOI
30. Long, D.; Liu, J.; Bai, L.; et al. Continuously selective photocatalytic CO_2 fixation via controllable S/Se ratio in a TiO_2-MoS*x*Se*y* dual-excitation heterostructured nanotree. *ACS. Photonics.* **2020**, *7*, 3394-400. DOI
31. Cho, I. S.; Chen, Z.; Forman, A. J.; et al. Branched TiO_2 nanorods for photoelectrochemical hydrogen production. *Nano. Lett.* **2011**, *11*, 4978-84. DOI
32. Cho, I. S.; Lee, C. H.; Feng, Y.; et al. Codoping titanium dioxide nanowires with tungsten and carbon for enhanced photoelectrochemical performance. *Nat. Commun.* **2013**, *4*, 1723. DOI
33. Bayan, E.; Lupeiko, T.; Pustovaya, L.; Volkova, M.; Butova, V.; Guda, A. Zn-F co-doped TiO_2 nanomaterials: synthesis, structure and photocatalytic activity. *J. Alloys. Compd.* **2020**, *822*, 153662. DOI
34. Cao, X.; Wen, P.; Ma, R.; et al. Ni_2P nanocrystals modification on Ta:α-Fe_2O_3 photoanode for efficient photoelectrochemical water splitting: In situ formation and synergistic catalysis of Ni_2P@NiOOH cocatalyst. *Chem. Eng. J.* **2022**, *449*, 137792. DOI
35. Zhang, K.; Jin, B.; Park, C.; et al. Black phosphorene as a hole extraction layer boosting solar water splitting of oxygen evolution catalysts. *Nat. Commun.* **2019**, *10*, 2001. DOI PubMed PMC

36. Dotan, H.; Sivula, K.; Grätzel, M.; Rothschild, A.; Warren, S. C. Probing the photoelectrochemical properties of hematite (α-Fe_2O_3) electrodes using hydrogen peroxide as a hole scavenger. *Energy. Environ. Sci.* **2011**, *4*, 958-64. DOI
37. Jia, H.; Shang, H.; He, Y.; et al. Engineering the defect distribution via boron doping in amorphous TiO_2 for robust photocatalytic NO removal. *Appl. Catal. B-Environ. Energy.* **2024**, *356*, 124239. DOI
38. Ma, J.; Liu, T.; Chen, G.; et al. Tuning the selectivity of photothermal CO_2 hydrogenation through photo-induced interaction between Ni nanoparticles and TiO_2. *Appl. Catal. B-. Environ.* **2024**, *344*, 123600. DOI
39. abstract: Angew Chem Int Ed. 40/2024. *Angew. Chem. Int. Ed.* **2024**, *63*, e202484011. DOI